Effects of the fidelity level of numerical simulations on the wake meandering phenomenon

IOP Conf. Series: Journal of Physics: Conf. Series **1256** (2019) 012010 doi:10.1088/1742-6596/1256/1/012010

Effects of the fidelity level of numerical simulations on the wake meandering phenomenon

N. Coudou[1,2,3], M. Moens[1], J. van Beeck[2], L. Bricteux[3], P. Chatelain[1]

[1]Institute of Mechanics, Materials and Civil Engineering, Université catholique de Louvain, 1348 Louvain-la-Neuve, Belgium
[2]von Karman Institute for Fluid Dynamics, 1640 Sint-Genesius-Rode, Belgium
[3]Mechanical Engineering Department, Université de Mons, 7000 Mons, Belgium

E-mail: nicolas.coudou@vki.ac.be

Abstract.

The aim of this paper is to verify that a modeling approach affordable at wind farm scale, in this case a fourth-order finite differences code combined with a rotating actuator disk, provides equivalent results in terms of wake meandering compared to a method with a higher fidelity level, i.e. a Vortex Particle-Mesh Method combined with immersed lifting lines. The analysis is performed on the wake centerlines obtained from Large Eddy Simulations of an isolated NREL 5-MW wind turbine subject to several synthetic turbulent inflows: 6%, 10%, and 15% turbulence intensity. A direct comparison of the wake centerlines reveals a good match between the two approaches up to five rotor diameters. Concerning the amplitude and wavelength of the wake meandering, the lower fidelity code leads to larger amplitudes and shorter wavelengths. Assuming that Taylor's frozen turbulence hypothesis is applicable, the Strouhal number St is computed as the ratio between the rotor diameter and the wavelength. Obtained values are such that $0.22 \leqslant St \leqslant 0.4$.

1. Introduction

Wind turbine wake meandering is a critical issue in wind farms as this oscillatory motion of the wakes increases fatigue loads on downstream machines and impacts their power production. The first step to study this phenomenon is to detect the wake centerline. Several methods for tracking of the wake centerline of an isolated wind turbine subject to a uniform inflow and a synthetic turbulent inflow were proposed in [1]. The simulations were performed with a state-of-the-art Vortex Particle-Mesh (VPM) method combined with immersed lifting lines. The most robust technique was then deployed inside a fourth-order finite differences (FD) code combined with rotating actuator disks (AD) to track individual wakes at wind farm scale. The robustness of this technique is here improved by means of an advection model to limit the search of the wake centroid to an area around its expected position.

The aim of the present paper is to verify that a modeling approach affordable at wind farm scale, in this case the FD code combined with rotating actuator disks, provides equivalent results in terms of wake centerline position compared to a higher level of fidelity, i.e. the VPM method combined with immersed lifting lines. To answer this question, we compare the wake centerlines obtained by both approaches for an isolated 5MW NREL wind turbine subject to

several synthetic turbulent inflows. The comparison is quantified through the study of the wake position signal in terms of amplitude, wavelength and frequency.

2. Wake centerline tracking algorithm

Among the algorithms tested in Coudou et al. [1], the most robust technique to perform run-time tracking of the wake centroid in a cross-flow plane located downwind of a machine subject to a turbulent inflow is based on the convolution

$$(y_c, z_c) = \text{argmax}\,(p * f_G) \tag{1}$$

between the available power density in the flow

$$p(y, z) = \frac{1}{2} u_x |\mathbf{u}|^2 \tag{2}$$

where u_x is the streamwise velocity component and $|\mathbf{u}|$ is the magnitude of the velocity vector, and a Gaussian masking function

$$f_G(y, z) = A \exp\left(- \left(\frac{(y - \mu_y)^2}{2\sigma_y^2} + \frac{(z - \mu_z)^2}{2\sigma_z^2} \right) \right) \tag{3}$$

with $A = -1$, $\mu_{y,z} = 0$, and $\sigma_{y,z} = 0.5D$. Note that $\sigma_{y,z}$ can be adapted automatically in space and time during the simulation through the implementation of a method based on Laplacian computation [1]. As it does not impact the wake centroid location, $\sigma_{y,z}$ was kept constant for this study to make easier the comparison between the two approaches tested.

Physically, this convolution method relies on the computation of the wind power inside a disk (with a Gaussian weighting) located in a cross-flow plane and with a diameter equal to the rotor diameter D. This disk center position can be shifted in $y-$ and $z-$directions; the wake center corresponds to the disk position for which the available power is minimum [2].

Finally, by tracking the wake centroid in several downwind cross-flow planes, the wake centerline can be obtained.

3. Numerical tools

3.1. Vortex Particle-Mesh (VPM) method

The Vortex Particle-Mesh method [3, 4, 5, 6] relies on the discretization of the velocity ($\mathbf{u}$)-vorticity ($\boldsymbol{\omega} = \nabla \times \mathbf{u}$) formulation of the incompressible Navier-Stokes equations in a Lagragian form. In this method, the vorticity field is discretized with particles which are used solely for the advection treatment, thereby avoiding dispersion errors and waiving classical time stability constraints, e.g. Courant number constraints. The use of a mesh along with the particles in the VPM method offers several advantages. The mesh enables the treatment of the Lagrangian distortion through the periodic regularization onto the grid of the particles set [6]. In addition, the mesh handles the computationally intensive tasks : the evaluation of differential operators and the use of fast Poisson solvers for the computation of velocity. Both discretisations communicate through high order interpolation.

This method is able to solve complex turbulent flows at high Reynolds number by using a Large Eddy Simulation (LES) approximation with a Regularized Variational Multiscale (RVM) subgrid-scale model [7] designed as an eddy viscosity model acting only on the small scales.

3.1.1. Blade modeling through immersed lifting lines The generation of vorticity along the rotor blades is accounted for through immersed lifting lines. Under the assumption of slender blades, a blade can be approximated as a concentrated bound vortex going through the quarter-chord line, and the flow around the airfoil can be treated as essentially two-dimensional in a section. For a steady flow, the lift per unit span $\mathbf{L}$ and the bound circulation $\mathbf{\Gamma}(r,t)$ are then related by the Kutta-Joukowski theorem

$$\mathbf{L} = \rho \mathbf{V}_{rel} \times \mathbf{\Gamma} \tag{4}$$

where ρ is the air density and $\mathbf{V}_{rel} = \mathbf{u} - \mathbf{u}_{blade}$ is the velocity relative to the blade. The lift can also be obtained from the relative velocity and the airfoil lift behavior, through its C_L coefficient –either static or in a dynamic stall model; this allows to compute the bound circulation $\mathbf{\Gamma}(r,t)$ as well as the shed vortex sheet from the solenoidal property of $\boldsymbol{\omega}$.

3.1.2. Turbulent inflow A turbulent velocity field $\mathbf{u}'$ is synthesized through Mann's algorithm [8]. In order to carry the turbulence into the domain through the inflow plane, this turbulent velocity field is translated into a set of vorticity particles, more adequate for the Lagrangian method used. Note that because of the unbounded conditions in the $y-$ and $z-$directions, this initially periodic velocity field is made compact through a smooth clipping along its edges.

3.1.3. Numerical setup The simulations are performed for an isolated NREL offshore 5-MW baseline wind turbine [9] operating at its optimum tip-speed ratio (TSR) of 7.55. Only the blades of the machine are modeled using immersed lifting lines. The spatial resolution is such that 32 points are used to model each blade. The computational domain initially extends over $14D \times 4D \times 4D$; the domain is unbounded in $y-$ and $z-$directions. Based on the spatial resolution of the blades, it leads to an initial grid with approximately 59 million nodes ($\Delta x = \Delta y = \Delta z \simeq 1.97$m). The wind turbine rotor is located $3D$ after the inlet and is subject to several turbulent inflows synthesized through Mann's algorithm [8] in a $26D \times 4D \times 4D$ box. The inflow velocity is $U_\infty = 9$ ms^{-1} in the $x-$direction and the turbulence intensities tested are $TI = u'/U_\infty = 6\%, 10\%$ and 15%. As the Mann algorithm is used to generate the inflow, the integral length scales are the same for the three turbulence intensities : $L_x = 1.35D$, $L_y = 0.23D$, and $L_z = 0.46D$; with the x-axis in streamwise direction, the y-axis in vertical direction and the z-axis in spanwise direction.

3.2. Fourth-order finite differences (FD) code
The VPM approach is well suited for high-fidelity and high-resolution simulations of an isolated wind turbine. However, it becomes unaffordable for simulations at wind farm scale for which another approach is required : LES on coarse meshes, performed using a fourth-order finite difference (FD) code [10]. In this code, instantaneous velocities are imposed at the inlet boundary and a convective boundary condition is applied at the outflow. Periodic boundary conditions are imposed in the spanwise direction and no-through flow is enforced at the top.

3.2.1. Blades modeling through advanced actuator disk (AD) The wind turbines are modeled with advanced AD, which account for thrust and torque effects; these disks also use the local prevailing velocities at every point of the AD for the computation of the aerodynamic loads [11, 12]. The model has been supplemented with a tip-loss correction based on a local estimation of the effective upstream velocity at every point of the AD [12].

3.2.2. Turbulent inflow The turbulent velocity fields $\mathbf{u}'$ are identical to those used for the VPM simulations.

3.2.3. Numerical setup Again, we consider the NREL-5MW machine at the same operating conditions. Only the blades of the machine are modeled using an advanced actuator disk. The domain size is $14D \times 9D \times 9D$ in order to be as close as possible to the unbounded conditions used in the VPM method. In order to evaluate whether the FD code could be a suitable tool to study wake meandering at wind farm scale, the resolution is kept to a typical resolution used for a wind farm : 16 points per rotor diameter ($\Delta x = \Delta y = \Delta z \simeq 7.88$m). The AD is located at $3D$ from the inlet and the inflow conditions are the same as those used for the VPM method.

4. Results

Figure 1 shows the wake centerlines, superimposed on snapshots of the velocity magnitude, obtained by the VPM method (solid line) and with the FD code (dash-dot line) in a horizontal plane at hub height for inflow turbulence intensities of $TI = 6\%$, $TI = 10\%$, and $TI = 15\%$. As it can be observed, the wake centerlines obtained clearly follow the wake motion. Qualitatively, there is a good agreement between the wake centerlines obtained by the two approaches up to five rotor diameters downstream the machine. Beyond this distance, the wake centerlines obtained by the FD code start to drift away from those obtained by the VPM method, especially as the inflow turbulence level increases.

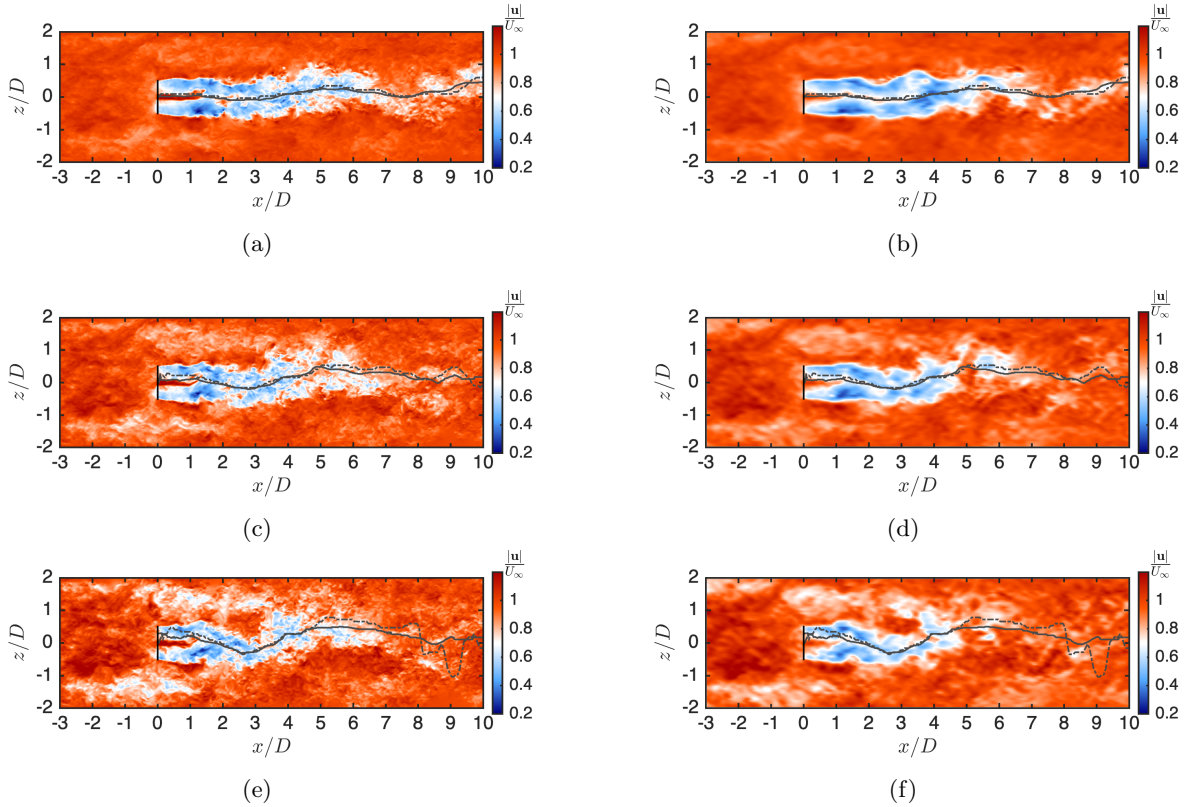

Figure 1. Snapshots in a horizontal plane at hub height of the velocity magnitude obtained by the VPM method ((a)-(c)-(e)) and the FD code ((b)-(d)-(f)) on which the wake centerlines obtained by VPM method (solid line) and with FD code (dash-dot line) are superimposed for several inflow turbulence intensities: $TI = 6\%$ ((a)-(b)), $TI = 10\%$ ((c)-(d)), and $TI = 15\%$ ((e)-(f))

In the next paragraphs, we aim to compare quantitatively the wake centerlines obtained by the two approaches. The statistics are computed from the data of 67 rotor revolutions, i.e.

approx. 28 convective times ($t^* = \frac{D}{U_\infty}$). These data are represented on Fig. 2 in a dimensionless manner as a function of space and time for the three inflow turbulence intensities tested. In order to obtain the wake centerline (i.e. wake centroid evolution as a function of space) at a specific time, one can simply extract the data along a horizontal line from Fig. 2. This is illustrated in Fig. 2 by the dashed lines corresponding to the time at which the wake centerlines presented on Fig. 1 were extracted. At the opposite, the data along a vertical line represent the evolution of the wake centroid as a function of time at a specific position behind the rotor. As it can be observed, the wake centroid motions obtained by the two approaches are similar in shape but vary in amplitude; the extrema being more pronounced with the FD code.

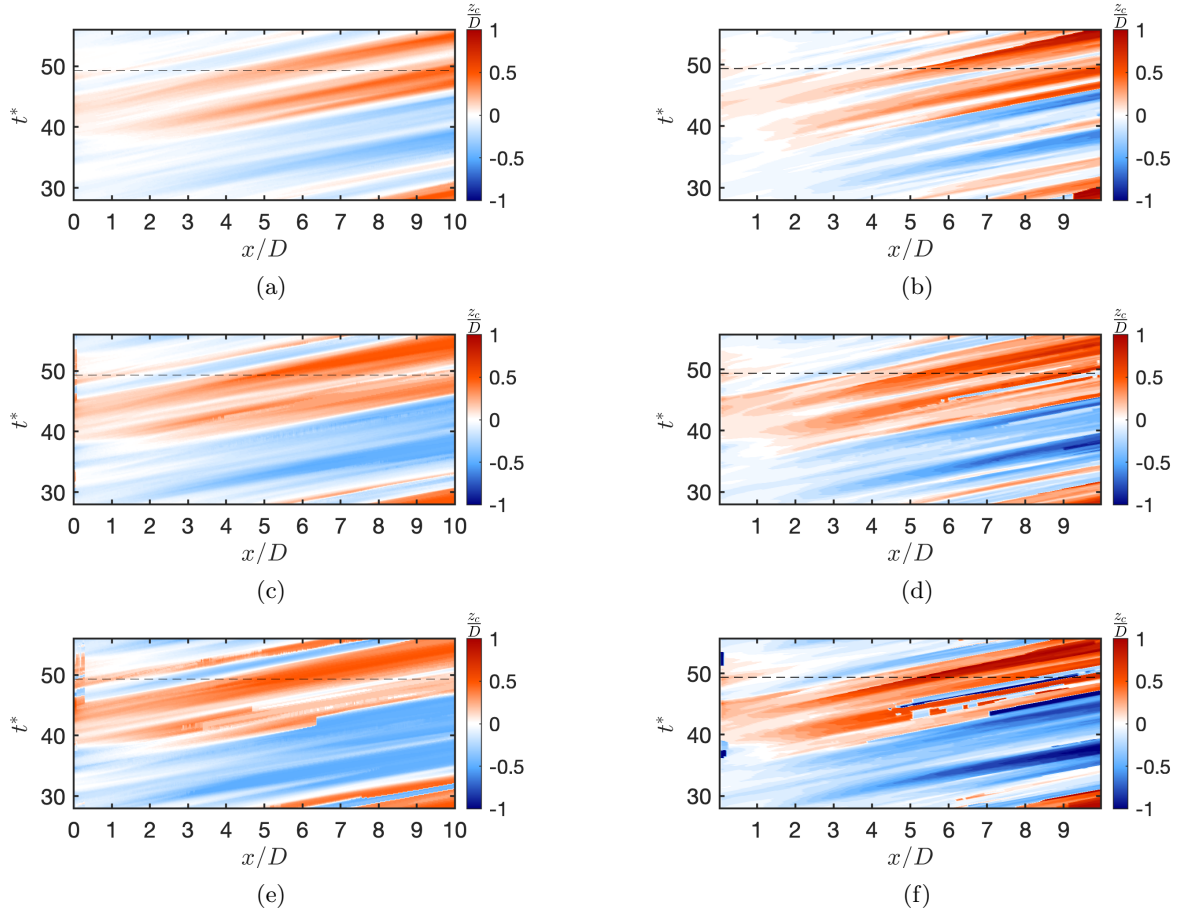

Figure 2. Dimensionless horizontal motion of the wake centerline as a function of space and time obtained by the VPM method ((a)-(c)-(e)) and the FD code ((b)-(d)-(f)) for several inflow turbulence intensities : $TI = 6\%$ ((a)-(b)), $TI = 10\%$ ((c)-(d)), and $TI = 15\%$ ((e)-(f))

The wake centerline envelopes (Fig. 3) were obtained by considering the maximum deflection of the wake centroid for each position behind the rotor. This is illustrated in Fig. 2 for the horizontal plane. Indeed, the maximum deflection of the wake centroid at a specific location corresponds to the maximum and minimum values along a vertical line located at the relevant position in Fig. 2. The wake centerline envelopes (Fig. 3) show that the maximum deflection of the wake centrelines increases with the downstream distance from the rotor. Furthermore, the maximum deviations of the wake centrelines obtained by the FD code are larger that those obtained by the VPM method, especially as the inflow turbulence intensity is larger. The fact that the extrema obtained with the FD code are larger than those obtained with the VPM

method is due to the lower spatial resolution and the larger diffusion of the FD simulations, making the wake centroid tracking more delicate. This difficulty is reinforced in the far wake and for the cases with a higher inflow turbulence level. Note that the peaks obtained just behind the rotor for $TI = 15\%$ are due to local maxima in the convolution leading to a biased wake centroid detection.

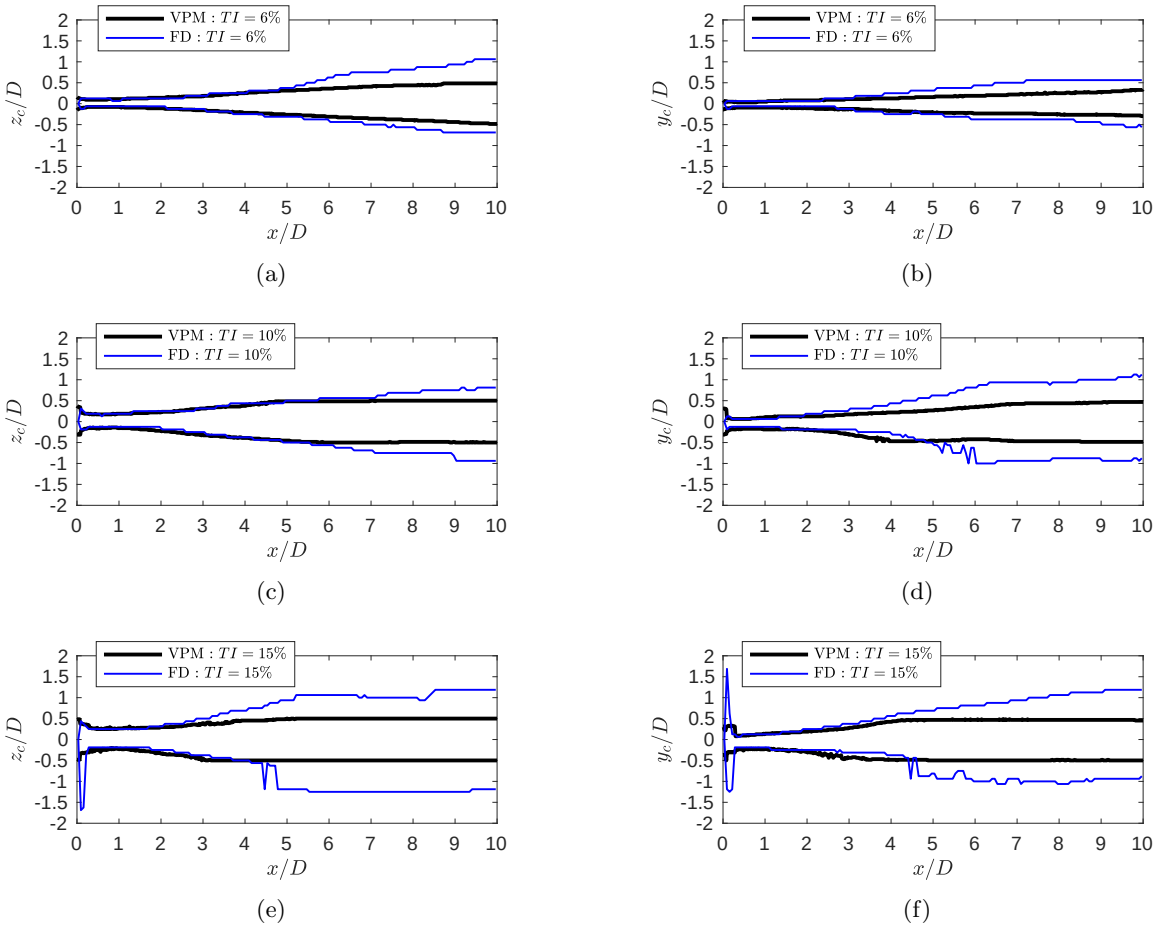

Figure 3. Dimensionless wake centerline envelopes obtained by the VPM method (thick black line) and the FD code (thin blue line) in a horizontal $(z - x)$ and in a vertical $(y - x)$ plane for several inflow turbulence intensities : $TI = 6\%$ ((a)-(b)), $TI = 10\%$ ((c)-(d)), and $TI = 15\%$ ((e)-(f))

Examining Fig. 4 reveals that the wake centroid distribution becomes larger with the downstream distance from the rotor and with the inflow turbulence level. Furthermore, one can observe that the wake meandering starts closer from the rotor when the inflow turbulence level increases. As it could be expected from the analysis of the wake centroid envelopes (Fig. 3), the distributions obtained with the FD code are wider compared to those obtained with the VPM code.

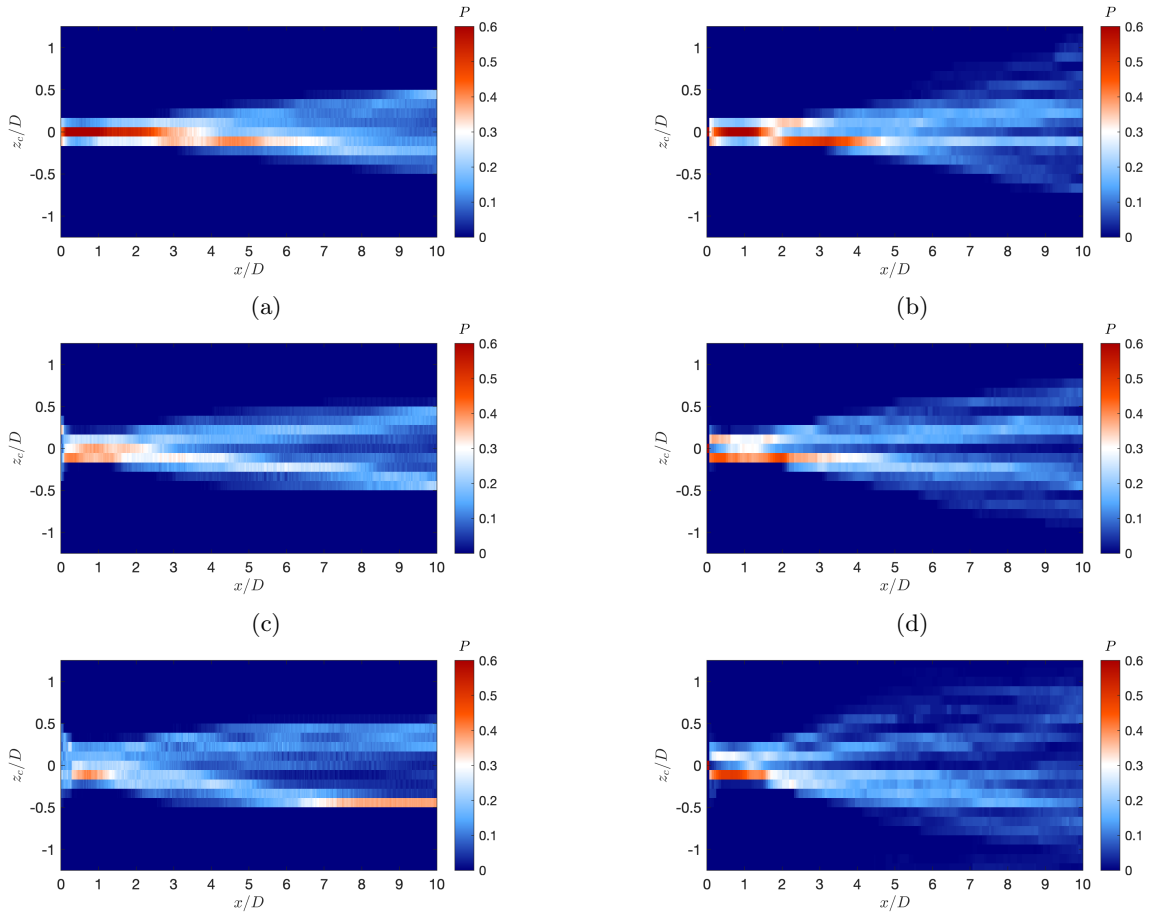

Figure 4. Probability of finding a wake centroid at a certain location in a horizontal plane at hub height in the wind turbine wake, obtained by the VPM method ((a)-(c)-(e)) and the FD code ((b)-(d)-(f)) for several inflow turbulence intensities : $TI = 6\%$ ((a)-(b)), $TI = 10\%$ ((c)-(d)), and $TI = 15\%$ ((e)-(f)), the bins width is $D/9$

In addition, a quantitative analysis of the wake centerline characteristics was performed on the basis of the work of Foti et al. [13]. In the following results, the amplitude of wake meandering is computed as half the cross-wind distance between consecutive maximum-minimum of the wake centerline while the wavelength is computed as the streamwise distance between two consecutive maxima or minima. The downstream position of these quantities was set to the intermediate position of the two points involved in the computation. The quantities were then binned, with respect to the downwind distance from the rotor, into half-diameter bins and the mean values were computed. The wake oscillations are captured in a horizontal plane at hub height and in a vertical plane passing through the hub ; even if the ground effect is not taken into account in the simulations, the inflow generated with the Mann algorithm is anisotropic, which should impact the wake meandering characteristics. Note that for the sake of transparency, downwind distances ranging from $0D$ to $10D$ are presented in Fig. 5 and 6, even if the exploitable part of the graphs is for $3 \lesssim x/D \lesssim 7$ because of the method used to determine the amplitude and wavelength of the oscillations.

Figures 5(a),(b) show the mean amplitude of the wake oscillations as a function of space. This

amplitude increases with the distance downwind from the rotor and with the inflow turbulence level. As expected with an anisotropic inflow, the wake meandering amplitudes are larger in the horizontal direction ($x-z$ plane) compared to the vertical direction ($x-y$ plane). Furthermore, the linear growth of the meandering amplitude with respect to the downwind distance from the rotor is highlighted on Fig. 5(c),(d), where the amplitude is normalized by the downstream distance. Indeed, the profiles are fairly constant in the central part of Fig. 5(c),(d). One can observe that the mean amplitude of the oscillations obtained by the VPM and FD methods are in good agreement and that the FD method leads to a larger amplitude overall. The obtained mean wavelengths of the oscillations are fairly constant for $3 \lesssim x/D \lesssim 7$ and range between $2.5D$ and $4.5D$ (Fig. 6). While there is no clear trend concerning the influence of the inflow turbulence level, the wavelengths obtained from the FD code are shorter than those obtained with the VPM method. The wavelengths are significantly larger than the mean integral length scales in the three directions : $2L_x \lesssim \lambda \lesssim 3L_x$, $12L_y \lesssim \lambda \lesssim 18L_y$, and $6L_z \lesssim \lambda \lesssim 9L_z$.

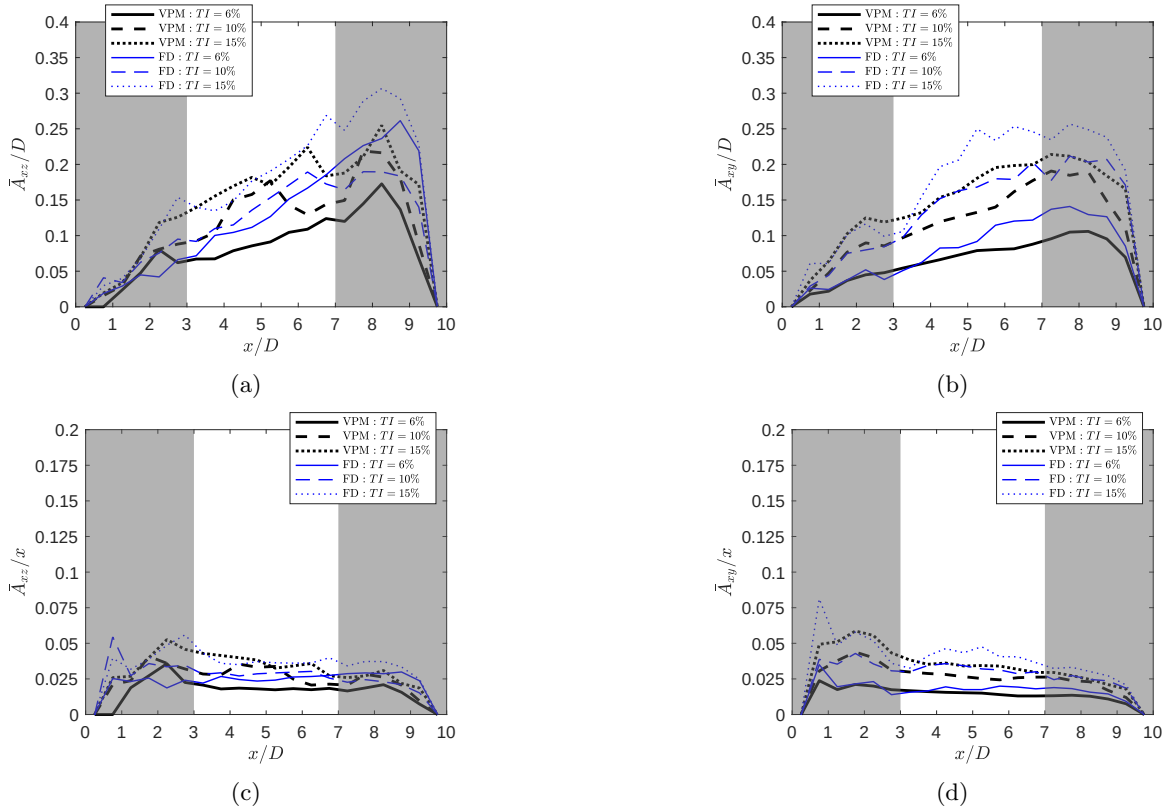

Figure 5. Mean binned wake centerlines amplitudes obtained by the VPM method (thick black line) and the FD code (thin blue line), in a horizontal ($z-x$) and in a vertical ($y-x$) plane, normalized by the rotor diameter ((a)-(b)) and by the downwind distance from the rotor ((c)-(d)), for several inflow turbulence intensities : $TI = 6\%$, $TI = 10\%$, and $TI = 15\%$; note that the exploitable part of the graphs ranges between $3 \lesssim x/D \lesssim 7$ because of the method used to determine the amplitude and wavelength of the oscillations

Assuming that Taylor's frozen turbulence hypothesis is applicable, the frequency can be computed from the wavelength.

$$f = \frac{U_\infty}{\lambda}, \tag{5}$$

and made dimensionless through the Strouhal number

$$St = \frac{fD}{U_\infty} = \frac{D}{\lambda}. \tag{6}$$

It leads to $0.22 \leqslant St \leqslant 0.4$ for $4.5D \geqslant \lambda \geqslant 2.5D$.

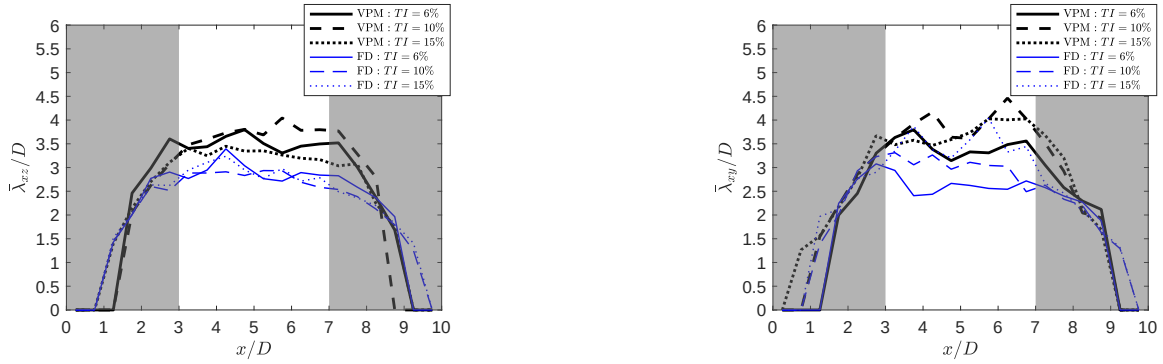

(a) (b)

Figure 6. Mean binned wake centerlines wavelengths obtained by the VPM method (thick black line) and the FD code (thin blue line), in a horizontal $(z-x)$ and in a vertical $(y-x)$ plane, normalized by the rotor diameter ((a)-(b)) for several inflow turbulence intensities : $TI = 6\%$, $TI = 10\%$, and $TI = 15\%$; note that the exploitable part of the graphs ranges between $3 \lesssim x/D \lesssim 7$ because of the method used to determine the amplitude and wavelength of the oscillations

5. Conclusions and perspectives

The aim of this work was to verify that a modeling approach affordable at wind farm scale, in this case a fourth-order FD code combined with an advanced rotating actuator disk, provides equivalent results in terms of wake meandering compared to a method with a higher fidelity level, i.e. a VPM method combined with immersed lifting lines. The comparison is performed for three inflow turbulence intensities, 5%, 10% and 15%. Even if the integral length scales play a major role in the wake meandering, this study highlights the influence of the turbulence intensity on the wake meandering characteristics independently of the integral length scales since they are identical whichever the turbulence level.

A direct comparison of the wake centerlines reveals a good agreement between the two approaches up to five rotor diameters downwind of the rotor. Beyond that distance, the wake centerlines obtained by the FD code start to drift away from those obtained by the VPM method, especially as the inflow turbulence level increases.

The wake centreline envelopes obtained by the FD code are larger that those obtained by the VPM method, especially for a larger inflow turbulence intensity or farther downwind from the rotor. This is partly caused by a less well defined wake within the FD code, because of a lower spatial resolution and larger diffusion, making the wake centroid tracking more delicate. This shows some limitation of the current tracking algorithm when it is used within the FD code.The wake centroids probability distributions obtained with the FD code are wider compared to those obtained with the VPM code. Furthermore, it was observed that the wake meandering starts closer to the rotor when the inflow turbulence level increases.

Concerning the amplitude of the wake meandering, it increases linearly with the distance from the rotor and increases also with the inflow turbulence level. Furthermore, a lower amplitude

was observed in the vertical plane because of the anisotropic inflow. Concerning the wavelengths, they are fairly constant and range between $2.5D$ and $4.5D$. Comparing both approaches, it was observed that the FD code tends to lead to larger amplitudes and shorter wavelengths than the VPM code. This study therefore shows that the tools used to perform the numerical simulations influence the wake meandering characteristics obtained. Eventually, Strouhal numbers ranging between 0.22 and 0.4 were obtained from the wavelengths using Taylor's frozen turbulence hypothesis.

The authors plan to run additional simulations with the FD code using the same spatial resolution as the VPM method to quantify the influence of the spatial resolution on the wake centerline tracking and therefore on the wake meandering characteristics. The next steps will be to improve the robustness of the tracking method for the wind farm simulation tool (the FD code). It should make it possible to study wake interactions and merging with the ultimate objective of performing wind farm control. A track that will be investigated to improve the robustness of the method is the use of a Kalman filter blending the wake centroids with the predictions of a simple wake advection model.

Acknowledgments

Nicolas Coudou is funded by the *Fonds pour la Formation à la Recherche dans l'Industrie et dans l'Agriculture (FRIA)*, Belgium. Preproduction runs were performed on computational resources provided by the Consortium des Équipements de Calcul Intensif (CÉCI), funded by the Fonds de la Recherche Scientifique de Belgique (F.R.S.-FNRS) under Grant No. 2.5020.11 and by the Walloon Region. The final simulations used computational resources made available on the Tier-1 supercomputer of the Fédération Wallonie-Bruxelles, infrastructure funded by the Walloon Region under the Grant Agreement No. 1117545.

References

[1] Coudou N, Moens M, Marichal Y, van Beeck J, Bricteux L and Chatelain P 2018 *Journal of Physics: Conference Series* **1037** 072024 URL `http://stacks.iop.org/1742-6596/1037/i=7/a=072024`
[2] Vollmer L, Steinfeld G, Heinemann D and Kühn M 2016 *Wind Energy Science* **1** 129–141
[3] Chatelain P, Curioni A, Bergdorf M, Rossinelli D, Andreoni W and Koumoutsakos P 2008 **197** 1296–1304
[4] Chatelain P, Backaert S, Winckelmans G and Kern S 2013 Large eddy simulation of wind turbine wakes *Proceedings of The 9th International Symposium on Engineering Turbulence Modelling and Measurements (ETMM-9), June 6–8, 2012, Thessaloniki, Greece* (*Flow, Turbulence and Combustion* vol 91) ed Rodi W ERCOFTAC (Springer) pp 587–605
[5] Backaert S, Chatelain P and Winckelmans G 2015 Vortex particle-mesh with immersed lifting lines for aerospace and wind engineering *Symposium on Particle Methods in Fluid Dynamics, October 15-17 2012, DTU Copenhagen* (*Procedia IUTAM* vol 18) ed Walther J H (IUTAM) pp 1–7
[6] Winckelmans G 2004 Vortex methods *Encyclopedia of Computational Mechanics* vol 3 ed Stein E, De Borst R and Hughes T J (John Wiley and Sons)
[7] Jeanmart H and Winckelmans G 2007 **19** 055110 ISSN 1070-6631
[8] Mann J 1998 *Probabilistic Engineering Mechanics* **13** 269–282 URL `http://www.sciencedirect.com/science/article/ pii/S0266892097000362`
[9] Jonkman J, Butterfield S, Musial W and Scott G 2009 Definition of a 5-mw reference wind turbine for offshore system development Tech. Rep. NREL/TP-500-38060 National Renewable Energy Laboratory (NREL)
[10] Duponcheel M, Bricteux L, Manconi M, Winckelmans G and Bartosiewicz Y 2014 *International Journal of Heat and Mass Transfer* **75** 470–482
[11] Moens M, Duponcheel M, Winckelmans G and Chatelain P 2016 *Journal of Physics: Conference Series* **753** 032053
[12] Moens M, Duponcheel M, Winckelmans G and Chatelain P *Wind Energy* Accepted for publication
[13] Foti D, Yang X and Sotiropoulos F 2018 *Journal of Fluid Mechanics* **842** 5–25